Article

Experimental Device to Evaluate Aerosol Dispersion in Venues

Isabell Schulz [1,2,*,†], Felix Hehnen [1,2,†], Kevin Harry Lausch [3], Sophia Mareike Geisler [4], Ümit Hasirci [2], Sophia Wolff [2], Tim Rese [1,2], Sebastian Schimek [5], Michael Lommel [2], Christian Oliver Paschereit [5], Stefan Moritz [4], Martin Kriegel [3] and Ulrich Kertzscher [1,2]

1   Biofluid Mechanics Laboratory, Institute of Computer-Assisted Cardiovascular Medicine, Deutsches Herzzentrum der Charité, 13353 Berlin, Germany; felix.hehnen@dhzc-charite.de (F.H.); tim.rese@charite.de (T.R.); ulrich.kertzscher@dhzc-charite.de (U.K.)
2   Charité–Universitätsmedizin Berlin, Corporate Member of Freie Universität Berlin and Humboldt-Universität zu Berlin, Charitéplatz 1, 10117 Berlin, Germany; uemit.hasirci@charite.de (Ü.H.); sophia.wolff@charite.de (S.W.); michael.lommel@charite.de (M.L.)
3   Hermann-Rietschel-Institut, Technical University of Berlin, 10587 Berlin, Germany; k.lausch@tu-berlin.de (K.H.L.); m.kriegel@tu-berlin.de (M.K.)
4   Section of Clinical Infectious Diseases, University Hospital Halle (Saale), 06120 Halle, Germany; mareike.geisler@uk-halle.de (S.M.G.); stefan.moritz@uk-halle.de (S.M.)
5   Institute of Fluid Dynamics and Technical Acoustics, Hermann-Föttinger-Institut, Chair of Fluid Dynamics, Technical University of Berlin, 10623 Berlin, Germany; schimek@tu-berlin.de (S.S.); oliver.paschereit@tu-berlin.de (C.O.P.)
*   Correspondence: isabell.schulz2@dhzc-charite.de
†   These authors contributed equally to this work.

Abstract: The COVID-19 pandemic has focused attention on the importance of understanding and mitigating the airborne transmission of pathogens in indoor environments. This study investigated the aerosol distribution in different indoor venues with varying ventilation concepts, including displacement, mixed, and natural ventilation. A measurement system was developed to investigate venue-specific aerosol distribution patterns using a sodium chloride solution as a tracer. To analyse the spatial dispersion of aerosols, Computational Fluid Dynamics (CFD) simulations were conducted in addition to experimental investigations. The investigations indicated the lowest aerosol load for the venue with displacement ventilation and the highest for the naturally ventilated venue. The measurement system developed in this study provides a useful tool for assessing the effectiveness of ventilation measures in reducing airborne transmission of pathogens in indoor environments. It also proved its wide range of applications, as it can be used in variously sized and shaped indoor environments, with or without an audience.

Keywords: aerosol dispersion; experimental measurement system; indoor environment; SARS-CoV-2

1. Introduction

The COVID-19 pandemic caused a significant public interest in reducing the risk of airborne transmission of pathogens, stimulating the investigation of the emission and transport of respiratory aerosols indoors [1]. The SARS-CoV-2 virus can be transmitted via aerosols released by breathing, speaking, sneezing, and coughing. The most common places for virus spreading are indoor environments [2] and the respiratory route is the primary mode of virus transmission [3]. Aerosols and droplets with a size of 2–5 μm carry the highest risk of an infection because these size droplets [4,5] have negligible sink velocities and follow any air flows accurately [6,7]. After evaporation, they can linger in still air for up to 60 min [8]. It is known that the implementation of appropriate ventilation measures can significantly reduce the risk of indoor infections [9]. Displacement ventilation aims to keep the fresh and polluted air separated [10]. A stream of fresh air from the floor is used to displace the waste air, which rises to the ceiling by buoyant force and is then removed from the room via air vents [11,12]. This creates two levels of air, with cool fresh

air in the occupied lower part of the room, and warm waste air in the unoccupied upper part of the room. Natural convection generates a cooling effect for the occupants, as the cool air rises and adsorbs the heat from them, which is then expelled from the room [13]. In a mixing ventilation system, fresh air is supplied to the room with a high initial mean velocity, creating a high turbulence intensity to promote good mixing of fresh and polluted air and an even distribution of temperature and pollutants throughout the venue [12,14]. Natural ventilation is a ventilation method where natural forces, such as wind and thermal buoyancy, drive outdoor air through purpose-built building envelope openings [15]. It is a ventilation method with very low investment and operating costs compared to mechanical ventilation systems. In addition, the effectiveness of natural ventilation on the infection risk potential and climatic conditions in the room is highly dependent on the outside temperature, the wind direction, and the user [16].

Developing methods to assess the risk of airborne pathogen transmission is essential to ensure that technologies used to control and improve air quality work effectively and efficiently [1]. For individualized considerations and high levels of accuracy, experimental studies must be conducted to examine the efficacy of ventilation measures [9]. Several strategies have been proposed for investigating aerosol distribution in indoor venues, each with its own advantages and limitations.

One method to directly detect SARS-CoV-2 in the air is active indoor air sampling followed by polymerase chain reaction (PCR) detection, as recently shown by Dinoi et al. [17]. While this method attempts to capture the actual viral load under real-world conditions, it does not provide controlled boundary conditions. Another method to evaluate the spread of aerosols is the use of tracer gases. A tracer gas is emitted into the venue and local concentrations are measured using infrared spectrometers [9]. This measurement technique is convenient for both small and large venues with outside air exchange. However, the room needs to be completely free from the tracer gas of potential previous measurements to avoid contamination. Also, tracer gases cannot be filtered, making this method unsuitable for evaluating air purifiers that rely on filtration [9]. A third method to observe how particles are transported in indoor environments is the surrogate particle method, where a particle generator is used for the emission of surrogate particles. Using optical particle counters or scanning mobility particle sizers at several positions allows the spatial and temporal measurement of particle numbers, concentration, and size distribution. For this, the room to be studied needs to be initially free of particles and all potential sources of particles, including humans. Consequently, this technique is not suitable for use in everyday environments [9]. Lommel and Froese et al. [18] developed a portable measurement system consisting of one aerosol generator and several aerosol absorbers. The aerosol generator continuously releases a 10% sodium chloride (NaCl) solution. The NaCl in the aerosol particles serves as a tracer, simulating the spread of an airborne virus [18]. The aerosol captured by the absorber is dissolved in ultrapure water and the amount of NaCl is calculated via conductivity measurement. Thus, the system can measure the temporal and spatial dispersion of the aerosol. It can be used to examine the effects of protective measures like active or passive ventilation and face masks without underlying assumptions or constraints like clean room environments.

In this paper, the measurement system of Lommel and Froese et al. [18] was modified. To investigate venue-specific aerosol distribution patterns, venues with different room characteristics and ventilation concepts were examined using the experimental measurement system and Computational Fluid Dynamics (CFD) analyses, with experimental methods being the focus of this paper. Three venues with different ventilation concepts were investigated, including displacement ventilation, mixing ventilation, and natural ventilation. The paper by Geisler and Lausch et al. [19] used the data of this study to investigate the infection risk potential in the venues, asses the effect of different mitigation measures, and develop recommendations. It also discusses the CFD simulations in more detail. All information about the setup and settings of the simulation can be found there. They are therefore not explicitly listed again in this publication. CFD data in this paper were used

to support and augment the experimental findings of the new measurement system. The combination of both methods gives a more complete picture and allows in some way for implications at points where no experimental measurements were made.

2. Materials and Methods

The study of venue-specific aerosol distribution patterns was examined by experimental and numerical measurements. The experimental investigation was conducted with an aerosol measurement system which consists of an aerosol generator and seven portable absorbers.

2.1. Aerosol Generator

The aerosol generator used for this study is the Atomizer Aerosol Generator ATM 230 (Topas GmbH, Dresden, Germany). The aerosol generator has an external compressed air supply (FK65 pro, 9 bar max, Weldinger, Oranienburg, Germany). It is also suitable for the generation of salt aerosols. The concentration of the NaCl solution used is decisive for the size of the resulting aerosol particles. Thus, the size distribution was measured by phase Doppler anemometry (PDA) [20] and the data were fitted through a t-location-scale distribution, which is useful for modelling data distributions with heavier tails than the normal distribution. The PDA measurements showed that at a nozzle pressure of 1.5 bar and a NaCl solution of 10% generate a particle size distribution that corresponds to that of sputum after evaporation (Figure A1) [21]. The emitted aerosol particles have a mean diameter of 2.4 µm with a standard deviation of 1.1 µm. This comes very close to the measured particle sizes of Lindsley et al. (d = 2.44 µm, standard deviation = 1.17 µm) [22]. Aerosols with a diameter <5 µm are of interest for the investigations because they can remain airborne for a long period of time under most indoor conditions and pathogens predominate in these aerosols [23]. Therefore, the tracer solution for the experiments was set to 10% NaCl in water. The NaCl within the emitted aerosol acts as a tracer particle. The aerosol is released with a controllable mass flow of 0.43 g min^{-1}. The aerosol generator operates in a continuous emission mode. The tracer solution is stored in a separate 5 L container and is pumped in a circuit between the atomizer container (500 mL filling volume) of the aerosol generator and the storage container with the aid of a peristaltic pump (DC 12 V, Vikye, Yiwu City, China). This ensures that the tracer solution has the same salt concentration throughout the dispersion and that the salt concentration of the tracer solution does not increase noticeably due to salt crystals which remain attached to the edge of the container. The tracer solution in the container is constantly heated to 37 °C.

2.2. Absorbers

The absorbers inhale the ambient air and measure the amount of inhaled NaCl. The design of the absorbers is illustrated in Figure 1. A vacuum pump (DC 12V 12W V, VN-C3 Mini, Vikye, China) generates a defined continuous volume flow through an inhalation tube. The volume of the aspiration air flow is 10 L min^{-1}. A fine filter (original coffee filter 1 × 6, Melitta, Minden, Germany) is attached to the end of the inhalation tube, surrounded by 150 mL of deionized water within a glass reservoir. The filter acts as an atomizer, breaking down the air stream into fine bubbles to dissolve the NaCl particles in the water. A peristaltic pump (DC 12 V, Vikye, Yiwu City, China) ensures that the filter is constantly flushed by pumping the water through a parallel circuit, in which a conductivity sensor (HI98192, Hanna Instruments, Vöhringen, Germany) is located. The conductivity sensor has a resolution of 0.01 µS/cm and a measurement accuracy of ±1%. The dissolved NaCl causes an increase in conductivity of the ultrapure water, enabling the determination of the NaCl amount. Therefore, when "aerosol amount" is mentioned in the experimental part of this paper, it only refers to the aerosol provided with the tracer NaCl. Other aerosols that may be present in the air are not considered.
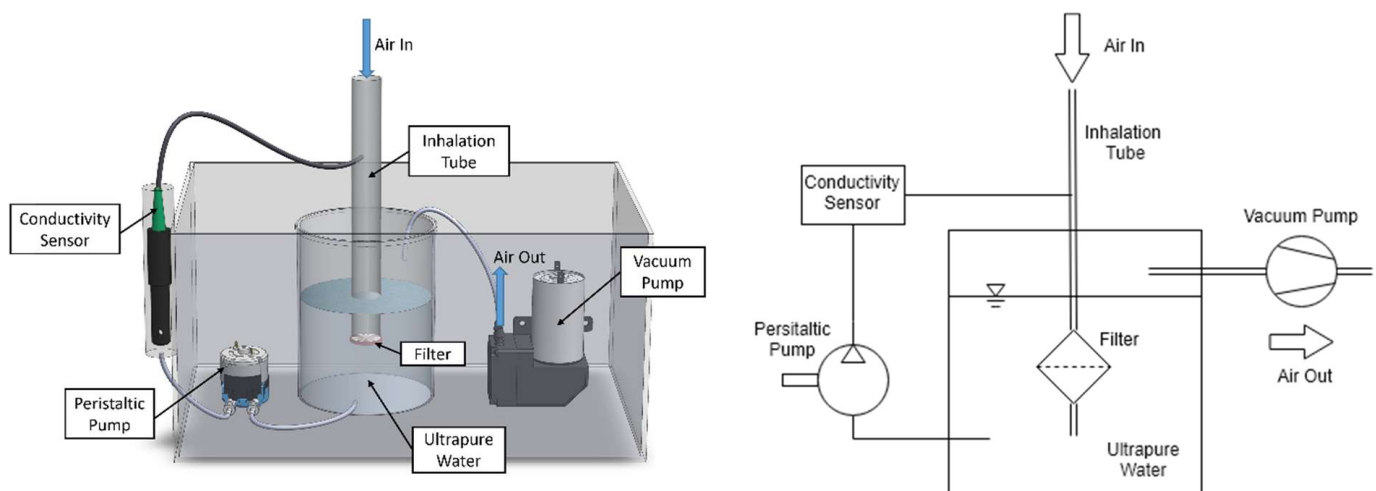
Figure 1. Illustration of an absorber: the aerosol is sucked through the inhalation tube into a closed reservoir filled with ultrapure water by a vacuum pump. The filter attached to the inhalation tube dissolves the NaCl particles in the ultrapure water. The ultrapure water is pumped through the sensor by a peristaltic pump.

2.3. Measurement Procedure

The measurements start with a lead-in time (I), which records current indoor air conditions in the absence of aerosol emissions by measuring the increase in conductivity inside the absorbers. Thus, in the first minutes of the measurement, the background concentration of conductive material in the air is measured. This slight increase in conductivity caused by the room-specific conductive aerosols or aerosols from previous measurements must be subtracted from the current measurement as an offset from the measured values during the post-processing. The lead-in time is also a good indicator of whether an environment has been sufficiently ventilated after previous measurements. Following the lead-in phase, the aerosol generator starts to release the tracer aerosols for a predetermined period of time. This phase is called the emission period (II). After the emission stops, the measurement is continued up to a predetermined time, called the lead-out time (III). During the entire measurement procedure (lead-in, emission, lead-out), which is displayed in Figure 2, the conductivity measurement of each individual absorber is recorded in real time on the measuring device. The conductivity sensor also continuously measures the temperature of the measuring fluid. The room temperature and humidity are recorded accordingly. Data were plotted and post-processed using Matlab (Version R2021a, MathWorks Inc., Natick, MA, USA). The post-processing included the temperature correction of the conductivity, the determination of aerosol concentrations in PPM from the conductivity, and the amount of salt emitted. The duration of the measurements at the individual venues varied, as the measurements were adapted to venue specific characteristics.

2.4. Measurement Setup

The aerosol generator and absorbers are positioned in different spatial arrangements to each other within the considered venue. The experimentally investigated seats were selected prior to the start of the CFD investigations and were chosen to the best of our knowledge to represent the aerosol distribution at the venue.

Venues can vary in terms of size and shape, ventilation system, and the arrangement of the audience. For smaller venues (up to 100 seats), the measurements were conducted with heat sources to mimic the buoyancy effects generated by humans, which significantly influence the room air flow. Heat sources have been used for smaller rooms as this allows us to be much more flexible with the number and duration of measurements. For an appropriate simulation of the volumetric flow rate of a human thermal plume (75 m^3/h) [24], heat sources were assembled consisting of a heating cable (80 W, Terra Exotica, Alfeld, Germany)

and a bucket that is placed on the heating cable with the opening facing downwards. The heat output corresponds to the physiological human heat emission for a low activity rate (80 W) [25,26]. The aerosol generator and the absorbers were placed on a heat source, whether measuring with or without an audience.
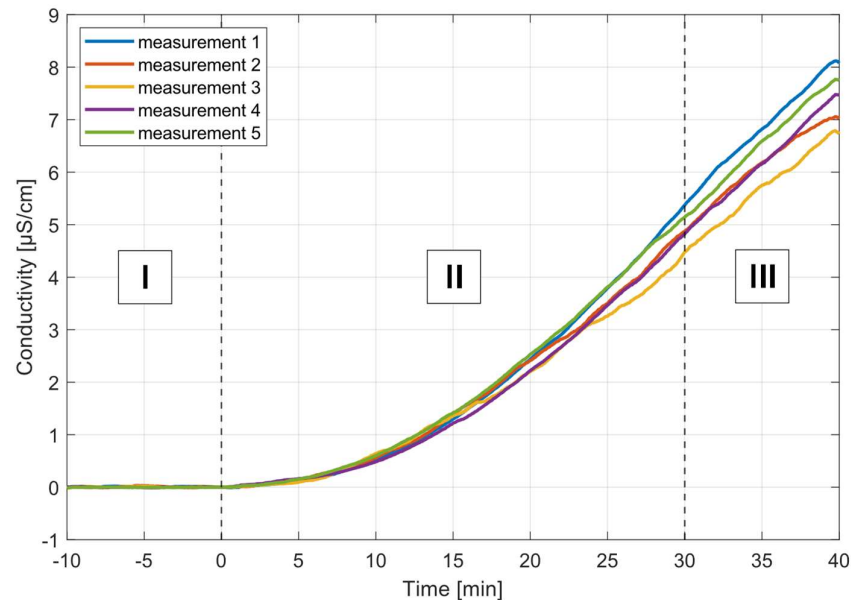

Figure 2. Increase in conductivity over time during a measurement procedure. The measurement procedure can be divided into three periods: lead-in (I), emission (II), and lead-out (III). Each measurement shows the mean value of the conductivity of all absorbers in the room. The lead-in time starts 10 min before the release of the aerosol. Then, the aerosol is released for 30 min and an increase in conductivity in the absorber can be observed. After 30 min, the aerosol release stops, and the increase in the conductivity slows down.

2.5. Reproducibility Measurements of the System

To prove that the system can reproducibly measure aerosol levels in rooms, the same measurement was repeated five times in a sealed conference room. This room has a volume of 100 m^3 and negligible air exchange. Two heaters constantly heat the room to $20 \pm 1\,^{\circ}$C. Due to thermal convection, there is a constant mixing of the room air in the entire room. Four absorbers were positioned at 1.5 m around the aerosol generator. The reproducibility measurement followed the measurement procedure stated above. A lead-in time of 10 min was chosen to sufficiently measure the background concentration of the NaCl particles. The aerosol was released by the aerosol generator for 30 min to ensure a high signal-to-noise ratio. The lead-out time was predetermined to 10 min. Therefore, the entire measurement time was 50 min.

2.6. Venues

All investigated rooms are indoor event locations. To investigate the venue-specific aerosol distribution patterns, venues with different room characteristics and ventilation systems (displacement ventilation, mixing ventilation, and natural ventilation) were examined.

2.6.1. Displacement Ventilation Venue (DVV)

The investigated DVV is a rectangular theatre with 99 seats, an ascending spectator area, and displacement ventilation. The air inlets are under the seats of row A to G and the air vents are on the upper left wall of the theatre (see Figure 3). Information about the room is presented in Table 1. The experimental measurements were performed without an audience and heat sources were used to mimic thermal buoyancy.
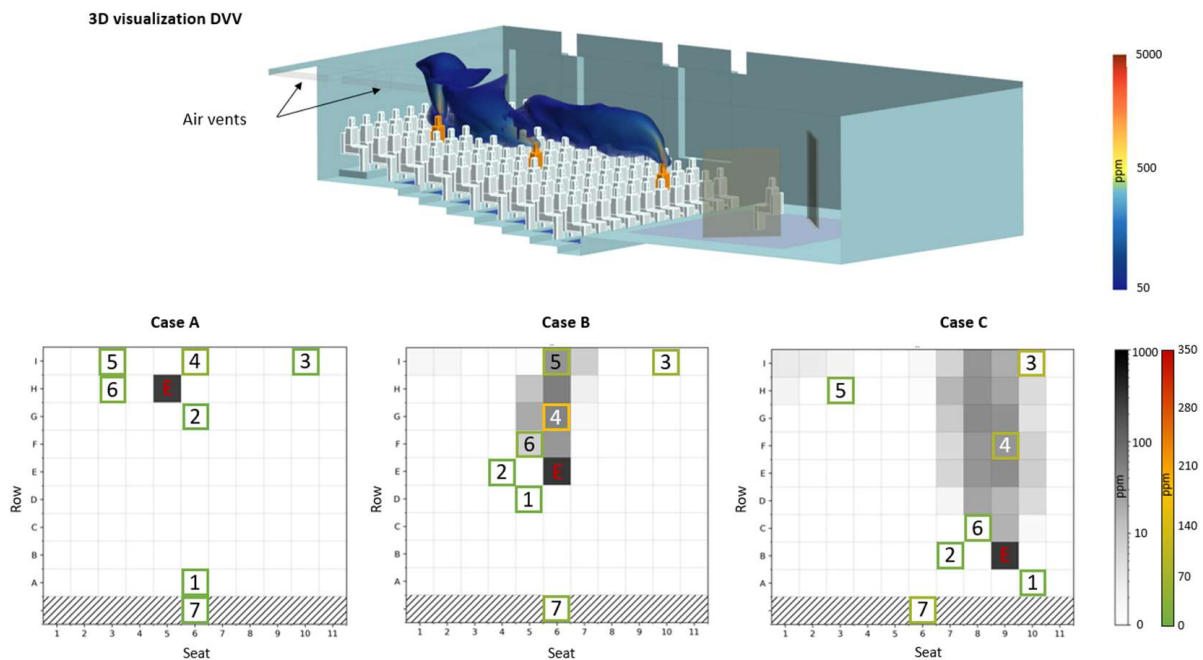
Figure 3. Experimental and simulated results of the three investigated emitter positions in the DVV. In the 3D visualization, the yellow dummies represent the positions of the aerosol generator measured with the experimental setup. Fresh air is inserted to the room under the seats and the polluted air is removed via air vents at the ceiling. The clouds over the yellow dummies show the aerosol plume dispersing in space calculated from numerical data. The three generator positions are: (Case A) aerosol generator in the back H5, (Case B) aerosol generator in the middle E6, and (Case C) aerosol generator in the front B9. E shows the position of the aerosol generator; numbers 1–7 the position of the absorbers. The colour of their frame indicates the amount of measured aerosol. During the measurements, heat sources were placed on the seats.

Table 1. Relevant parameter of the measurements in the DVV.

Quantity	Value	Quantity	Value
Ventilation type	displacement ventilation	Room temperature	$22.5 \pm 0.7\,^\circ$C
Room volume	530 m^2	Spectator area	ascending
Seats	99	Exposition time	60 min
Ceiling height	3.9 m	Audience	no
Supply air volume flow	4500 m^3/h	Date	25–27 October 2021

2.6.2. Mixing Ventilation Venue (MVV)

The MVV has 103 seats, which are arranged in a three-stage arena shape. The audience is seated on the floor (see Figure 4). Further information is available in Table 2. The measurements were performed with heat sources to mimic an audience.

Table 2. Relevant parameter of the measurements in the MVV.

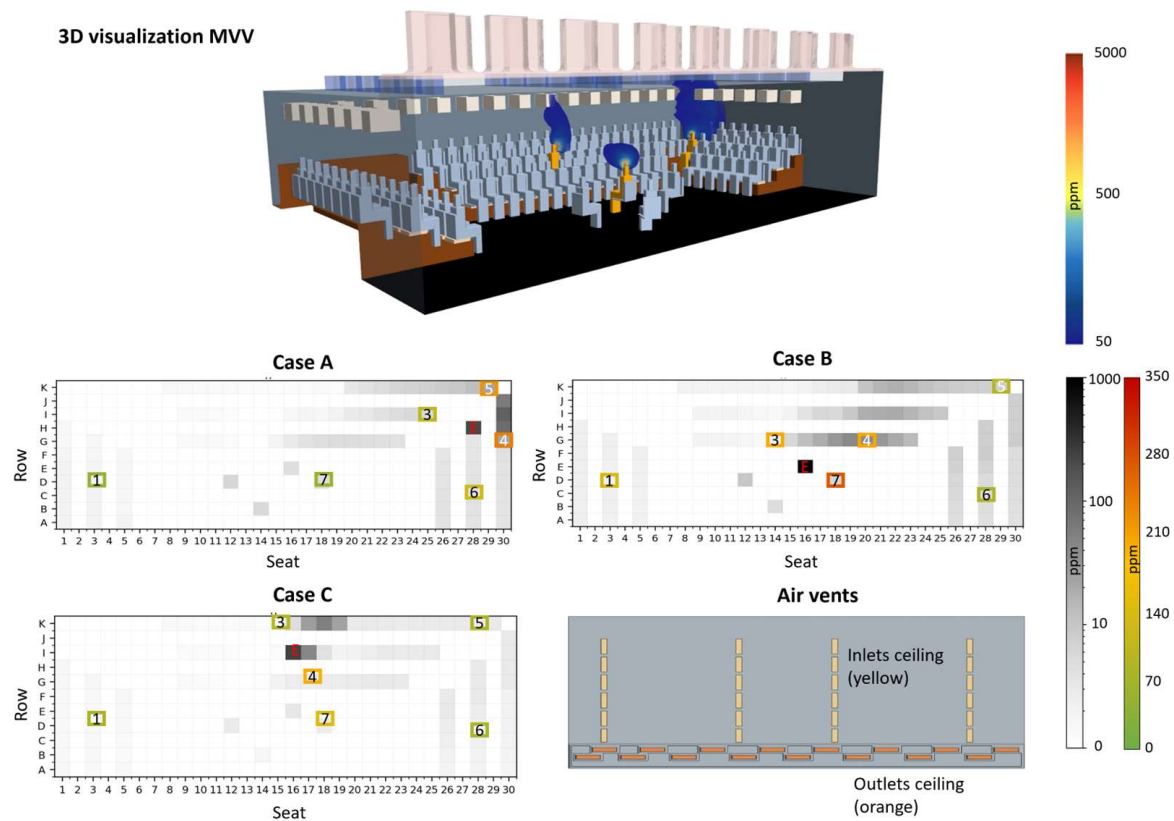| Quantity	Value	Quantity	Value
Ventilation type	mixing ventilation	Room Temperature	$25.35 \pm 3.15\,^\circ$C
Room volume	400 m^3	Spectator area	two stage, arena shape
Seats	103	Exposition time	45 min
Ceiling height	3.3 m	Audience	no
Supply air volume flow	6400 m^3/h	Date	12–13 January 2022

Figure 4. Experimental and simulated results of the three investigated emitter positions in the MVV. In the 3D visualization, the yellow dummies represent the positions of the aerosol generator measured with the experimental setup. A schematic representation of the air vents is shown (bottom right). The ventilation inlets are displayed in yellow and the ventilation outlets in orange. Both are located at the ceiling. The clouds over the yellow dummies show the simulated aerosol plume. The three generator positions are: (Case A) aerosol generator on the right H29, (Case B) aerosol generator on the stage E14, and (Case C) aerosol generator in the back I16. E shows the position of the aerosol generator; numbers 1–7 the position of the absorbers. The colour of their frame indicates the amount of measured aerosol. Unfortunately, absorber 2 experienced a malfunction and is therefore missing in the results.

2.6.3. Natural Ventilation Venue (NVV)

In the venue with natural ventilation (NVV), air can only be exchanged through open doors and a smoke vent. Therefore, the air exchange is not quantifiable due to its strong dependence on thermal and external boundary conditions. The venue has 240 seats and an ascending spectator area (see Figure 5). Further information is available in Table 3. The measurement in this venue was conducted during a dress rehearsal with a real audience, so only one aerosol generator position could be investigated.

Table 3. Relevant parameter of the measurements in the NVV.

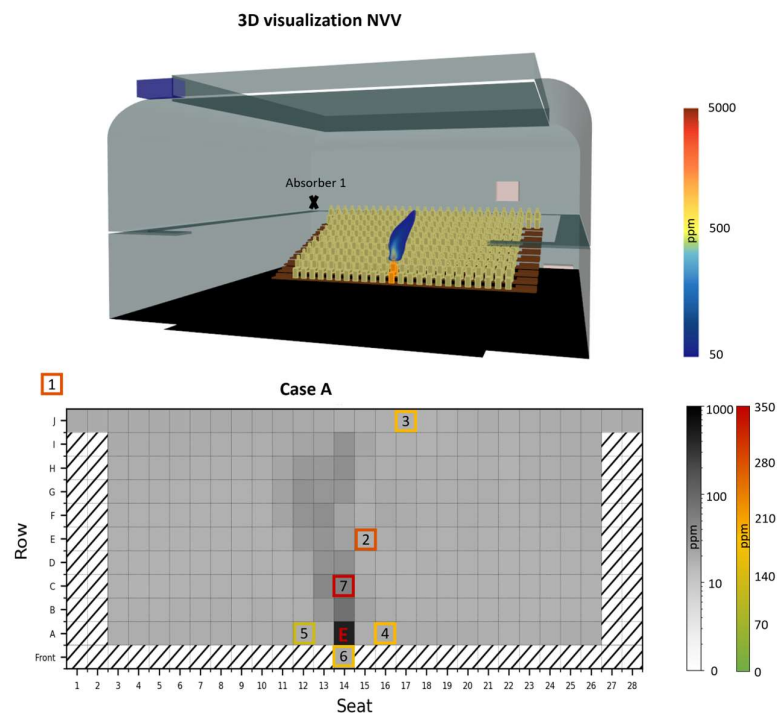| Quantity	Value	Quantity	Value
Ventilation type	natural ventilation	Room temperature	$19 \pm 0.5\,°C$
Room volume	6000 m^3	Spectator area	ascending
Seats	240	Exposition time	30 min
Ceiling heigh	12.8 m	Audience	yes
Supply air volume flow	unknown	Date	24 November 2021

Figure 5. Experimental and simulated results of the NVV. In the 3D visualization, the yellow dummy represents the position of the aerosol generator measured with the experimental setup. The cloud over the yellow dummy is showing the aerosol plume dispersing in space, calculated from numerical data. In Case A, the aerosol generator is positioned in the first row A14. E shows the position of the aerosol generator; numbers 1–7 the position of the absorbers. Absorber 1 is marked with a black cross in the 3D visualisation to indicate its position.

2.7. CFD Simulations

To support the experimental measurements and to arrive at a full understanding of the aerosol distribution in the venues, CFD simulations were performed. The non-isothermal, steady-state CFD simulations of the three venues were conducted on unstructured grids using Simcenter™ STAR-CCM+ (version 2021.2-2310). The modelling of the venues closely followed construction plans, walkthroughs, and additional information from the technical staff on site. Heat sources such as persons (assumed 80 W each), lighting, and production equipment were remodelled to match the measurement configuration. Supply air and the outside temperature were chosen based on the conditions at the day of the respective experiments. Further boundary conditions are added in Table A1. The mesh design relied on base sizes between 0.1 m and 0.3 m, with local refinements throughout the venue but especially close to heated or geometrically complex surfaces, and 4–6 prism layers were applied to support the near-wall modelling. In total, grid sizes ranged from 3.5 to 12 million finite volume cells. Mesh sensitivity was analysed for one venue (DVV) of the project where the passive scalar, temperature, TKE and momentum monitor values for three grids of increasing refinement (with base sizes of 5 cm, 10 cm, 20 cm) were observed. The differences in these monitor values were increasingly insignificant. Therefore, we chose the medium mesh density at the 10 cm base size (including prism layers and local refinements) as a reasonable trade-off. Air was treated as an incompressible, ideal gas where buoyancy effects were directly determined by the gravity model. Transport equations of flow and energy were solved with a segregated solver using the SIMPLE algorithm. Grey thermal, surface-to-surface radiation was used in combination with the segregated fluid temperature model. The realizable K-ε-model with a two-Layer formulation (Wolfstein) was applied as a two-equation RANS-model. Simplified mouth regions model the inlets of the tracer aerosol, where momentum-free passive scalars enter the fluid domain. For each emitting person (equivalent to aerosol generator), a separate passive scalar equation was solved.

The volume-averaged concentrations of the respective tracer within the hemispherical volume around the absorber's mouths (r = 0.23 m) were calculated and compared to the corresponding experimental value. Since the experiments relate the absorbed amount of NaCl to the emitted amount, a similar approach was chosen for the evaluation of the steady-state absorption of the tracer aerosol.

3. Results

The venue is displayed in a two-dimensional form as a matrix. To obtain aerosol distribution data for every position in the audience, CFD analyses were conducted. The numerical results are shown in shades of grey on a scale from 0 to 1000 ppm. The experimental results are obtained at seven selected seats by the measurement system. The results of the measurements are represented by a colour-coded outline of the seat on a colour scale with values from 0 to 350 ppm.

3.1. Reproducibility Measurements of the System

Figure 2 shows the results of the reproducibility measurements. The mean values of the four absorbers are compared over time. At 30 min after the start of the aerosol release, a mean conductivity of μ = 4.92 μS/cm was detected with a standard variation of σ = 0.34. After 40 min, the mean conductivity was μ = 7.41 μS/cm with a standard variation of σ = 0.54. Thus, the signal-to-noise-ratio (SNR) after 30 min is:

$$\text{SNR} = \frac{\mu}{\sigma} = \frac{4.92}{0.34} = 14.47$$

3.2. Displacement Ventilation Venue

The influence of the positioning of the aerosol generator on the aerosol distribution was investigated in the DVV for the three cases A, B, and C. In A, the aerosol generator was placed in the back row (seat H5), in B it was placed in the middle row (seat E6), and in C in the second row of the spectator area (seat B9) (Figure 3).

Table 4 shows the results of this investigation. The position of the aerosol generator has a decisive influence on the distribution of aerosols in the venue. In the CFD data, it can be seen that an aerosol plume forms behind the aerosol generator. The further forward in the audience the aerosol generator is placed, the more seats are affected by the plume and thus the higher the aerosol load in the venue. This trend can also be found in the experimental results.

Table 4. Experimental results of the investigations in the DVV.

Absorber		1	2	3	4	5	6	7
Aerosol	A	0	7	10	38	15	4	0
amount	B	2	8	27	177	68	33	41
[ppm]	C	10	6	88	79	22	6	46

The experimentally derived amount of aerosol is highest in B and lowest in A (Table 4), B and C show an increased measured aerosol amount at the positions directly behind the aerosol generator (absorbers 4, 5), while the positions next to (absorber 2) and in front (absorber 1) of the aerosol generator were characterised by a low aerosol absorption. In B and C, the absorber four seats behind the aerosol generator still absorbs around an order of magnitude more aerosol than absorbers 1 and 2. The highest measured value can be found in the position two seats behind the absorber (B, absorber 4).

3.3. Mixing Ventilation Venue

The influence of the positioning of the aerosol generator on the aerosol distribution was investigated in the MVV for the three cases A, B, and C. In A, the aerosol generator

was placed on the right (seat H28), in B it was placed on the stage (seat E16), and in C in the back (seat I16). The results of this investigation are shown in Figure 4 and Table 5. In A, the highest aerosol amounts are measured by absorbers 4 and 5, the positions closest to the aerosol generator. Absorbers 3 and 6, which are also located near the aerosol generator, absorb a significant amount of aerosol. The same pattern can be observed for B and C. The three absorbers closest to the aerosol generator measure the highest amounts of aerosol. In both cases, the three absorbers placed further away from the aerosol generator together sampled about one third of the total aerosol measured. The total amount of measured aerosol by the six absorbers is the highest in B. Absorber 2 unfortunately failed to collect measurements due to a technical defect.

Table 5. Experimental results of the investigations in the MVV. Malfunction of Absorber 2 during the measurements.

Absorber		1	2	3	4	5	6	7
	A	51	-	100	257	220	132	65
Aerosol amount [ppm]	B	138	-	197	198	111	88	269
	C	77	-	117	185	85	99	147

3.4. Natural Ventilation Venue

For this venue only, one position was examined, where the emitter is placed in the middle of the front row (seat A14). The results of this investigation are shown in Figure 5 and Table 6. The highest amount of aerosol was measured with absorbers 7 and 2, just behind the aerosol generator. Both the experimental and simulation data again show the formation of an aerosol plume which is directed from the aerosol generator backwards over the audience. Even absorbers 1 and 3, which were located significantly further behind the aerosol generator, absorbed considerably more aerosol than the three absorbers in front (6) and next to the aerosol generator (4, 5). The latter absorbed only half as much aerosol as the most heavily exposed absorber, absorber 7, two seats behind the aerosol generator. Both the experimental and numerical results show that, in contrast to the DVV, the entire venue is highly loaded with aerosols. In the CFD, there is no position with low amounts of aerosol.

Table 6. Experimental results of the investigations in the NVV.

Absorber	1	2	3	4	5	6	7
Aerosol amount [ppm]	270	271	182	177	132	160	345

The high aerosol load measured by absorber 1 is notable. This absorber was placed outside of the spectator area slightly above the highest spectator rank at the level of the theatre lighting. Since the theatrical fog had accumulated as a layer predominantly at this height, it was considered an interesting position to measure the aerosol exposure.

3.5. Comparison of the Venues

In Figure 6, all measurements are shown in a boxplot. Even though a representative aerosol load cannot be determined from only seven measurement points in the room, a trend can be identified. The total aerosol load is significantly lower in the DVV than in the NVV.
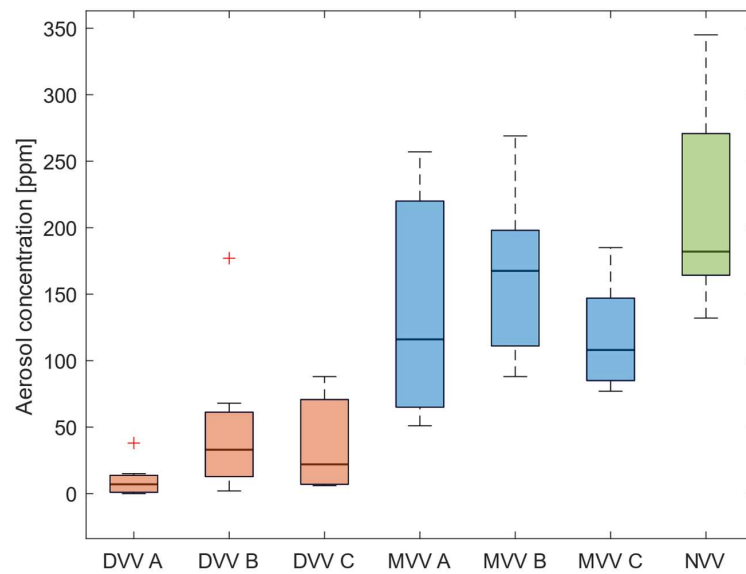
Figure 6. Comparison of the absorbed amount of aerosol at each measurement. The total aerosol load is significantly lower in the DVV than in the NVV. It should be noted that each boxplot consists of a maximum of 7 different measurement positions and therefore does not represent the total aerosol load in the room with sufficient accuracy. Red crosses represent outliers (outside 1.5 times the interquartile range).

By comparing the dispersion characteristics of the aerosol in the different rooms, the DVV and NVV show similar dispersion patterns of the aerosol plume. This aerosol plume forms behind the aerosol generator over the audience. Absorbers inside this plume measure multiple times higher aerosol loads compared to absorbers outside the plume. For the mixing ventilation, a different dispersion pattern can be observed. A clear negative correlation between the measured aerosol and the distance to the emitter can be seen in Figure 7. All absorbers of the three MVV measurements are shown as a scatter plot. The aerosol amount decreases with increasing distance from the absorbers. This relationship can be described with a power law (Figure 7, black dashed curve, $f(x) = a \times b$, $a = 228.8$, $b = -0.418$, R-square = 0.51).
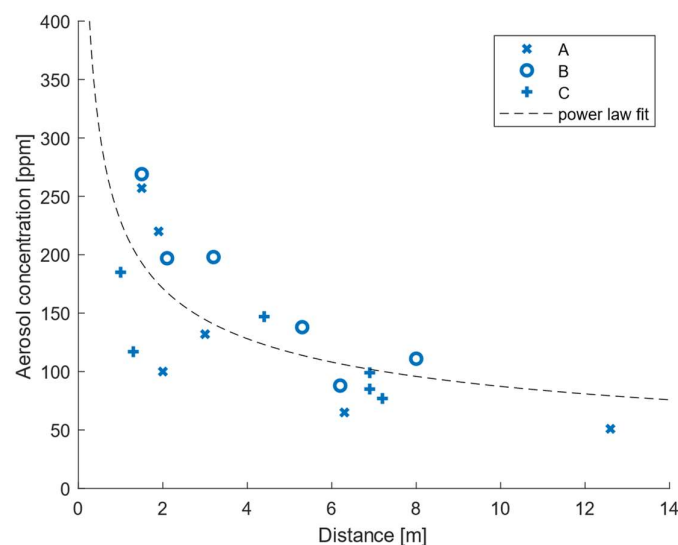

Figure 7. In the MVV, the aerosol amount decreases with increasing distance from the absorbers. This relationship can be described with a power law (black curve, $f(x) = a \times x^b$, $a = 228.8$, $b = -0.418$, R-square = 0.51).

3.6. Comparison of Experimental Measurements and CFD Simulations

Figure 8 shows the normalised amount of aerosol taken up by each absorber for both the experimental measurements and the CFD results. The consistency of data from experiments and simulations depends on the venue. For the DVV (orange), there are two groups of data points—the absorbers in the aerosol plume (upper-right, orange), and the absorbers outside the aerosol plume (lower-left, orange). For both groups, the data match quite well, although outside the aerosol plume slightly more aerosol was measured experimentally than numerically. The DVV values give an R-square value of 0.8633 when compared to the perfect match (black dashed diagonal). For the MVV, the data match less well than for the DVV. Across all three measurements, the match of the values deviates notably more than for the DVV and NVV, with an R-square value of −0.1845. For the NVV, the experimental and simulation data match with an R-square value of 0.5155.
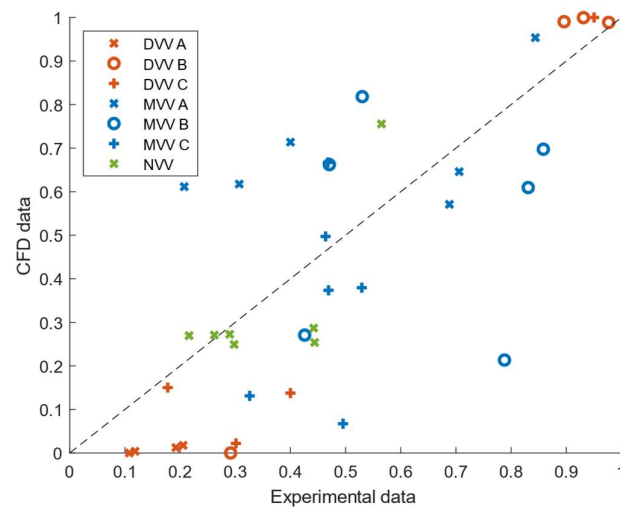

Figure 8. Comparison of normalized data points from CFD simulation and experimental measurements. Each colour represents a different venue. The *x*-axis shows the total aerosol load from the experimental measurements, the *y*-axis the total load from the simulations. For better comparability, all values were normalized. The closer the values are to the black dashed line, the better the agreement between experiment and simulation. R-square values for the values compared to the perfect agreement (black dashed line): DVV R-square = 0.8633, MVV R-Square = −0.1845 and NVV R-Square = 0.5155.

4. Discussion

Case studies worldwide indicate that airborne aerosols are a major transmission route for SARS-CoV-2 virus indoors [27,28]. So far, most COVID-19 risk evaluations for indoor environments are based on calculations applying spreadsheet models including relevant environmental and physiological parameters [29,30]. The typical settings to evaluate the infection risk represent classrooms or office spaces with space volumes below 400 m^3 and fewer than 50 persons present [31].

The DVV, with an ascending spectator area, represents good ventilation of the venue in all three scenarios, indicated by the low amount of absorbed aerosols. However, the observed aerosol plume was associated with highly exposed positions behind the aerosol generator, while the positions in front of and next to the aerosol generator remained almost unaffected, creating characteristic areas of low and high exposure. The position of the aerosol generator has a huge impact on the size of the aerosol plume and, therefore, on the aerosol exposure in the venue, as can be seen in Figure 3 between the rear position A and the front position C. The CFD data indicated that the further in front of the ascending spectator area that the aerosol generator is placed, the higher the aerosol load in the entire venue. This can be explained by the positioning of the aerosol generator in close proximity to the air vents (Figure 3 Case A), directly exhausting the emitted plume through the air

vents. This observation is not supported by the experimental data, since in case C, a lower aerosol load is observed than in case B, despite a greater distance to the exhaust (Figure 6). However, this is possibly due to the unfortunate positioning of the absorbers. Only one absorber was positioned directly in the aerosol plume, so it is difficult to make a statement about the total aerosol load in the room.

It seems that the room air flow of the DVV can be reproduced well with CFD simulations. Qualitatively, the distribution of aerosols in the simulation and the experiments match well. A closer look at the numbers shows that the high aerosol loads are overestimated by the simulation and the low ones are underestimated. However, numerical simulations seemed to adequately reproduce experimentally derived aerosol distribution patterns for DVV and are therefore a useful tool for aerosol distribution analysis when experimental measurements are not possible.

For the MVV, the total amount of aerosol measured by the absorbers was 77%, higher than that in the DVV. In contrast to the DVV and NVV, it was observed that the amount of aerosol decreases with increasing distance from the emitter (Figure 7). This behaviour, which is shown in Figure 7, does not correspond to the common idea of ideal mixing ventilation, in which the air is uniformly mixed throughout the room. However, predicting highly exposed positions is more difficult because the air flow in the mixing ventilation venue is less directional and not dominated by strong thermal buoyancy. It is therefore less predictable and appears to react sensitively to marginal changes in boundary conditions. This might also be the reason for the poor match of the experimental and simulated data. It seems that the less-predictable air flow in the MVV cannot be reproduced by the CFD simulation to match the experimental results. However, the higher aerosol load in the MVV compared to the DVV was shown in both experiments and CFD simulations.

The aerosol plume of the NVV behind the aerosol generator is wider and laterally less confined compared to DVV-C, which represents a similar emitter position. The measured amount of aerosol within the venue is much higher than the measured values at the other rooms, which is also confirmed by the CFD data. Similarly, current studies have shown that the risk of airborne transmission does not correlate with increasing distance in naturally ventilated venues, as the highest probabilities of infection were observed at greater distances [32,33]. Even though there is no mechanical ventilation in the NVV, a very characteristic air flow is formed by the buoyancy above the spectators, which is also shown by CFD simulation, indicating good agreement between numerical and experimental data.

In Table 7 a summary of the characteristics of the three investigated venues based on experimental measurements and CFD analysis is shown.

Table 7. Summary of the characteristics of the three investigated venues based on experimental measurements and CFD analyses.

	Displacement Ventilation Venue	**Mixing Ventilation Venue**	**Natural Ventilation Venue**
Aerosol distribution	Aerosol plume pulling backwards over the emitter	No dominant room air flow, depending on boundary conditions Dispersion in the entire venue	Aerosol plume pulling backwards over the emitter
Positions with high aerosol exposure	Along the aerosol plume	Forecast only possible to a limited extent	Along the aerosol plume Prediction only possible to a limited extent
Aerosol load of the venue	Low outside of the aerosol plume	Medium, depending on the distance to the aerosol generator	High in the whole venue and highest inside of the aerosol plume

4.1. Features and Advantages of the Measurement System

A major advantage of the measurement system is its wide range of applications. In contrast to other available measurement methods, it is not limited to clean rooms. The

measurement system can perform in variously sized and shaped indoor environments, with or without audience. If the measurements are conducted without an audience, heat sources are used, ensuring a higher reproducibility compared to measurements with a human audience. It needs to be emphasized that parameters such as room temperature, relative humidity, and fluid turbulence influence the range and time aerosols are suspended in air [27,31,34]. For these reasons, measurement results can vary with the slightest change in the boundary conditions. However, this also applies to dispersion of pathogenic aerosol in a real case. This paper focuses on fully occupied venues where the occupants are static most of the time. The measurement system can also be used in other ways, but the results are less reproducible if the air flow is influenced by a strong movement of people.

Since a NaCl solution is used as a tracer, the system is not harmful when used with an audience. A limitation might occur in environments where the air contains a certain concentration of conductive particles similar to the emitted tracer solution. Nevertheless, the background concentration of particles is measured anew for each measurement. Whether a room has been fully ventilated after a measurement or whether a background concentration is present can be deduced from a change in the increase in conductivity during the lead-in time, which is then subtracted from the total increase.

To obtain the most meaningful measurement output, the positioning of the absorbers and aerosol generator at the venue is essential. Whether a tracer reaches a certain absorber in a certain time depends on the flow field. To obtain a good first impression of the global air flow for application in rooms with complex air flow, it is helpful to perform a smoke dispersion analysis before the measurements. Subsequently, particularly critical areas can be analysed by the aerosol generator and the absorbers. The measuring system can also be used to investigate the influence of hygiene measures [18], to show the influence of the supply air volume flow and to show the effect of the occupancy of an venue [19].

4.2. Limitations

As the experimental measurement system only covers seven positions at the venue, it is currently not possible to representatively map the air flow of the room. It is difficult to select a representative configuration of the aerosol generator and absorber positions to cover the full range of sites with low and high aerosol amounts. Since the time for the measurements in the venues was limited for various reasons, our focus was to consider different aerosol generator positions to properly investigate the flow in the room. The reliability of the experimental data could be improved by using more absorbers and repeated measurements.

5. Conclusions

In summary, the measuring system has shown that it is capable to examine venues of different sizes and characteristics making predictions about the aerosol distribution and aerosol load in the room. Due to its portability, it can be used on site. It can measure in real time. The experimental measurements allow for the examination of the effects of protective measurements like different ventilation strategies without underlying assumptions or restrictions like clean room environments.

The more the air flow in a venue is dominated by strong effects such as mechanical ventilation or thermal buoyancy, the better this can be reproduced through CFD simulations. For such venues, the experimental and simulative results showed good agreement. Here the experimental measurement system can offer a good possibility to validate CFD simulations. In venues with complicated undefined air flows, CFD simulations and many experimental measurement systems often cannot provide sufficiently reproducible data. For the fast and reliable evaluation of the dispersion of aerosols in such spaces, experimental systems such as our measurement system remain the primary option.
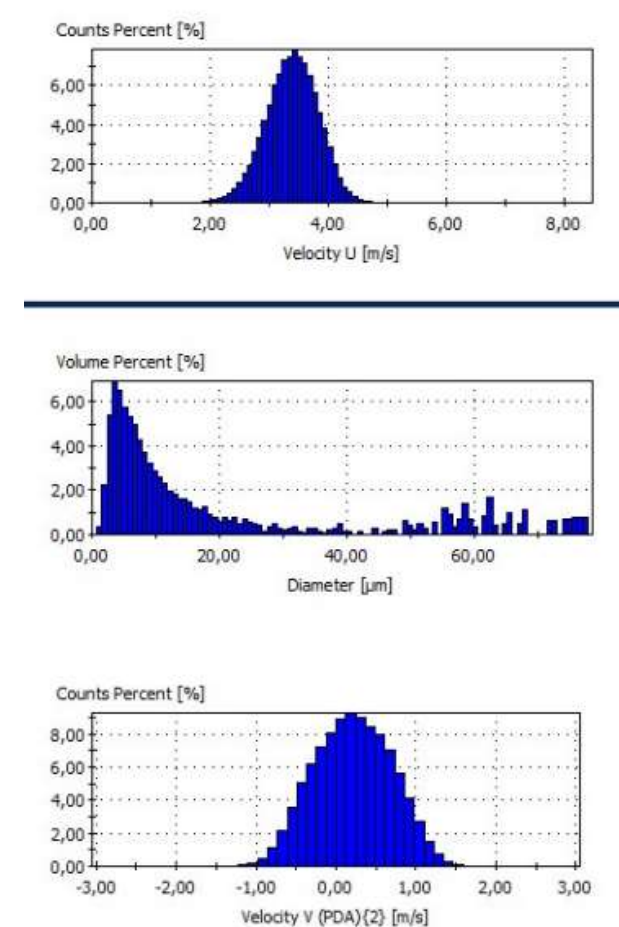
Appendix A

Figure A1. Results of the PDA measurement of the Topas ATM 230 with a 10% NaCl solution at 37 °C with different pressures.

Appendix B

Table A1. Selected boundary conditions for the chosen venues, DVV, MVV, NVV. Supply air mass flow for the MVV and NVV is derived from volume flow, 6400 m^3/h and 1500 m^3/h, respectively.

Boundary Condition/Venue	DVV		MVV	NVV
Inlet Temperature	18 °C		17 °C	20 °C
CSP Heat Flow	c. 80 W			
Lighting Heat Flow	c. 3600 W		c. 10,000 W	c. 0 W
Additional Heat Sources	c. 400 W		c. 550 W	c. 0 W
Supply Air Mass Flow	1.5 kg/s		2.162015 kg/s	0.5016408 kg/s
Tracer injection (Mouth)	momentum-free, normalized to averaged emission value			
Additional Boundary Condition (Convection Wall)	Outer Wall	Windows	Outer Wall	Inner Wall
- Ambient Temperature	10 °C	10 °C	3 °C	18 °C
- Heat Transfer Coefficient	25.0 W/(m^{2}K)	25.0 W/(m^{2}K)	25.0 W/(m^{2}K)	1.0 W/(m^{2}K)
- (Multi-Layer) Thermal Resistance, Conductivity	1 Layer, 0.48 m, 0.7 W/(mK)	0.74 m^{2}K/W	1 Layer, 0.48 m, 0.7 W/(mK)	1 Layer, 0.6 m, 0.7 W/(mK)
Inlets: Turbulence Intensity	0.01		0.05	0.01
Inlets: Turb. Viscosity Ratio	10			

References

1. Arvelo, I.; Pagone, F.; Persky, J.; Carpio, C.E.; Arnold, P.; Clements, N. Decay rates of two tracer gases compared to DNA-tagged liquid aerosol tracer particles: Impact of varying dilution rate and filtration. *Build. Environ.* **2022**, *212*, 108819. [CrossRef]
2. Qian, H.; Miao, T.; Liu, L.; Zheng, X.; Luo, D.; Li, Y. Indoor transmission of SARS-CoV-2. *Indoor Air* **2021**, *31*, 639–645. [CrossRef] [PubMed]
3. Kriegel, M.; Hartmann, A.; Buchholz, U.; Seifried, J.; Baumgarte, S.; Gastmeier, P. SARS-CoV-2 aerosol transmission indoors: A closer look at viral load, infectivity, the effectiveness of preventive measures and a simple approach for practical recommendations. *Int. J. Environ. Res. Public Health* **2022**, *19*, 220. [CrossRef] [PubMed]
4. Mao, N.; An, C.K.; Guo, L.Y.; Wang, M.; Guo, L.; Guo, S.R.; Long, E.S. Transmission risk of infectious droplets in physical spreading process at different times: A review. *Build. Environ.* **2020**, *185*, 107307. [CrossRef] [PubMed]
5. Morawska, L.; Johnson, G.R.; Ristovski, Z.D.; Hargreaves, M.; Mengersen, K.; Corbett, S.; Chao, C.Y.; Li, Y. Size distribution and sites of origin of droplets expelled during expiratory activities. *J. Aerosol Sci.* **2009**, *40*, 256–269. Available online: http://eprints.qut.edu.au/ (accessed on 23 June 2024). [CrossRef]
6. Zeng, G.; Chen, L.; Yuan, H.; Yamamoto, A.; Maruyama, S. Evaporation flow characteristics of airborne sputum droplets with solid fraction: Effects of humidity field evolutions. *Phys. Fluids* **2021**, *33*, 123308. [CrossRef] [PubMed]
7. Löhner, R.; Antil, H. High fidelity modeling of aerosol pathogen propagation in built environments with moving pedestrians. *Int. J. Numer. Method. Biomed. Eng.* **2021**, *37*, e3428. [CrossRef]
8. Vuorinen, V.; Aarnio, M.; Alava, M.; Alopaeus, V.; Atanasova, N.; Auvinen, M.; Balasubramanian, N.; Bordbar, H.; Erästö, P.; Grande, R. Modelling aerosol transport and virus exposure with numerical simulations in relation to SARS-CoV-2 transmission by inhalation indoors. *Saf. Sci.* **2020**, *130*, 104866. [CrossRef]
9. Siebler, L.; Calandri, M.; Rathje, T.; Stergiaropoulos, K. Experimental Methods of Investigating Airborne Indoor Virus-Transmissions Adapted to Several Ventilation Measures. *Int. J. Environ. Res. Public Health* **2022**, *19*, 11300. [CrossRef]
10. Ye, W.; Pan, Y.; He, L.; Chen, B.; Liu, J.; Gao, J.; Wang, Y.; Yang, Y. Design with modeling techniques. In *Industrial Ventilation Design Guidebook: Volume 2: Engineering Design and Applications*, 2nd ed.; Elsevier: Amsterdam, The Netherlands, 2021; pp. 109–183. [CrossRef]
11. Skistad, H.; Mundt, E.; Nielsen, P.V.; Hagström, K.; Railio, J. *Displacement Ventilation in Non-Industrial Premises-REHVA Guidebook*; Rehva: Ixelles, Belgium, 2002.
12. Shan, X.; Zhou, J.; Chang VW, C.; Yang, E.H. Comparing mixing and displacement ventilation in tutorial rooms: Students' thermal comfort, sick building syndromes, and short-term performance. *Build. Environ.* **2016**, *102*, 128–137. [CrossRef]
13. Sinopoli, J. Heating, Ventilating, and Air Conditioning Systems. In *Smart Building Systems for Architects, Owners and Builders*; Eslevier: Amsterdam, The Netherlands, 2010; pp. 31–46. [CrossRef]
14. Li, A.; Kosonen, R.; Hagström, K. Industrial ventilation design method. In *Industrial Ventilation Design Guidebook: Volume 1 Fundamentals*, 2nd ed.; Elsevier: Amsterdam, The Netherlands, 2020; pp. 19–37. [CrossRef]

15. Atkinson, J. *World Health Organization. Natural Ventilation for Infection Control in Health-Care Settings*; World Health Organization: Geneva, Switzerland, 2009.

16. Seifert, J. *Repetitorium Raumlufttechnik*; VDE-Verlag: Berlin, Germany, 2014.

17. Dinoi, A.; Feltracco, M.; Chirizzi, D.; Trabucco, S.; Conte, M.; Gregoris, E.; Barbaro, E.; La Bella, G.; Ciccarese, G.; Belosi, F. A review on measurements of SARS-CoV-2 genetic material in air in outdoor and indoor environments: Implication for airborne transmission. *Sci. Total Environ.* **2022**, *809*, 151137. [CrossRef]

18. Lommel, M.; Froese, V.; Sieber, M.; Jentzsch, M.; Bierewirtz, T.; Hasirci, Ü.; Rese, T.; Seefeldt, J.; Schimek, S.; Kertzscher, U. Novel measurement system for respiratory aerosols and droplets in indoor environments. *Indoor Air* **2021**, *31*, 1860–1873. [CrossRef] [PubMed]

19. Geisler, S.M.; Lausch, K.; Hehnen, F.; Schulz, I.; Kertzscher, U.; Kriegel, M.; Paschereit, C.O.; Schimek, S.; Hasirci, Ü.; Brockmann, G. Airborne infection risk in venues with different ventilation strategies—A comparison between experimental, numerical and analytical approaches. *medRxiv* **2023**. [CrossRef]

20. Mayinger, F.; Feldmann, O. *Optical Measurements*; Verlag: Berlin, Germany, 2001. [CrossRef]

21. Lindsley, W.G.; Pearce, T.A.; Hudnall, J.B.; Davis, K.A.; Davis, S.M.; Fisher, M.A.; Khakoo, R.; Palmer, J.E.; Clark, K.E. Quantity and size distribution of cough-generated aerosol particles produced by influenza patients during and after illness. *J. Occup. Environ. Hyg.* **2012**, *9*, 443–449. [CrossRef] [PubMed]

22. Fennelly, K.P. Particle sizes of infectious aerosols: Implications for infection control. *Lancet Respir. Med.* **2020**, *8*, 914–924. [CrossRef] [PubMed]

23. Craven, B.A.; Settles, G.S. A computational and experimental investigation of the human thermal plume. *J. Fluids Eng. Trans. ASME* **2006**, *128*, 1251–1258. [CrossRef]

24. Kumar, R.; Aggarwal, R.K. Full Length Research Article Predicting Energy Requirement for Heating the Building Using Artificial Neural Network. *Int. J. Dev. Res.* **2013**, *3*, 10–14. Available online: http://www.journalijdr.com (accessed on 23 June 2024).

25. Sessler, D.I.; Schroeder, M. Heat Loss in Humans Covered with Cotton Hospital Blankets. *Anesth. Analg.* **1993**, *77*, 73–77. [CrossRef]

26. Xie, X.; Li, Y.; Chwang AT, Y.; Ho, P.L.; Seto, W.H. How far droplets can move in indoor environments-revisiting the Wells evaporation-falling curve. *Indoor Air* **2007**, *17*, 211–225. [CrossRef] [PubMed]

27. Zenit, R.; Feng, J.J. Hydrodynamic Interactions Among Bubbles, Drops, and Particles in Non-Newtonian Liquids. *Annu. Rev. Fluid Mech.* **2018**, *50*, 505–539. [CrossRef]

28. Kriegel, M.; Buchholz, U.; Gastmeier, P.; Bischoff, P.; Abdelgawad, I.; Hartmann, A. Predicted Infection Risk for Aerosol Transmission of SARS-CoV-2. *medRxiv* **2020**. [CrossRef]

29. Lelieveld, J.; Helleis, F.; Borrmann, S.; Cheng, Y.; Drewnick, F.; Haug, G.; Klimach, T.; Sciare, J.; Su, H. Model calculations of aerosol transmission and infection risk of COVID-19 in indoor environments. *Int. J. Environ. Res. Public Health* **2020**, *17*, 8114. [CrossRef] [PubMed]

30. Schade, W.; Reimer, V.; Seipenbusch, M.; Willer, U. Experimental investigation of aerosol and co2 dispersion for evaluation of COVID-19 infection risk in a concert hall. *Int. J. Environ. Res. Public Health* **2021**, *18*, 3037. [CrossRef] [PubMed]

31. Foster, A.; Kinzel, M. Estimating COVID-19 exposure in a classroom setting: A comparison between mathematical and numerical models. *Phys. Fluids* **2021**, *33*, 021904. [CrossRef]

32. Motamedi, H.; Shirzadi, M.; Tominaga, Y.; Mirzaei, P.A. CFD modeling of airborne pathogen transmission of COVID-19 in confined spaces under different ventilation strategies. *Sustain. Cities Soc.* **2022**, *76*, 103397. [CrossRef] [PubMed]

33. Ai, Z.T.; Melikov, A.K. Airborne spread of expiratory droplet nuclei between the occupants of indoor environments: A review. *Indoor Air* **2018**, *28*, 500–524. [CrossRef] [PubMed]

34. Kalliomäki, P.; Saarinen, P.; Tang, J.W.; Koskela, H. Airflow patterns through single hinged and sliding doors in hospital isolation rooms. *Int. J. Vent.* **2015**, *14*, 111–126. [CrossRef]